IEEE Access
Multidisciplinary | Rapid Review | Open Access Journal

Received August 26, 2017, accepted September 19, 2017, date of publication September 26, 2017,
date of current version October 25, 2017.

Digital Object Identifier 10.1109/ACCESS.2017.2756672

A Compact UHF Antenna Based on Complementary Fractal Technique

FENG WANG[1], FENG BIN[1], QIUQIN SUN[1], JINGMIN FAN[1], AND HUISHENG YE[2]
[1]College of Electrical and Information Engineering, Hunan University, Changsha 410082, China
[2]Equipment Condition Assessment Center, Hunan Electric Power Research Institute, Changsha 410000, China

Corresponding author: Qiuqin Sun (sunqq@hnu.edu.cn)

This work was supported by the National Natural Science Foundation of China under Grant 51677061 and Grant 51507058.

ABSTRACT A compact and wideband ultra-high-frequency antenna is developed in this paper. By applying the Minkowski fractal geometry into both the lateral boundaries of monopole and the upper boundary of ground plane and loading the asymmetric strips at the top of monopole simultaneously, the miniaturization is realized; by means of adjusting the fractal direction to produce a complementary structure and cutting the triangular notch on the ground plane, the impedance bandwidth is enhanced. The influences of critical parameters on the impedance bandwidth are determined through the sensitivity analysis. Furthermore, to validate the performance of the proposed antenna, the return loss, radiation patterns, transfer function, and fidelity factors are measured; the electrical dimension and ratio bandwidth are compared with those of the existing antennas. It shows that the antenna with size of $0.28\lambda_L \times 0.28\lambda_L$ can cover the frequency ranging from 700 MHz to 4.71 GHz and has an average gain of 3.93 dBi along with strong pulse handling capability. The results demonstrate the superiority of the complementary fractal technique.

INDEX TERMS Compact antenna, complementary structure, fractal direction, ultra-high-frequency (UHF) antenna.

I. INTRODUCTION

Partial discharge (PD) is a common local dielectric breakdown phenomenon of an electrical insulation system, and it often takes place in gas-insulated switchgears, power transformers, switch cabinets, power cables, etc [1], [2]. A partial discharge is normally accompanied by electromagnetic (EM) and acoustic emissions [3]. Correspondingly, a number of methods have been proposed to detect them. Compared with ultrasonic detection and pulse current detection, the UHF method possesses the advantage of high sensitivity and strong anti-interference capability. Thus, it has drawn increasing attention over past decades [4]. The UHF antenna is a critical component and it plays a key role in the accuracy of the measurement system.

Various multiband UHF antennas have been developed so far. In general, the frequency of EM waves arising from PD varies from 300 MHz to 3 GHz, and the ratio bandwidth reaches up to 10:1. The existing multiband antennas, such as Hilbert fractal antenna [1] and modified loop antenna [2], only cover part of frequency band of PD signal. To address this issue, several improved broadband antennas, e.g., planar equiangular spiral antenna [3], horn antenna [4], and biconical log-periodic antenna [4], are sometimes employed. However, these antennas suffer from the excessive size, and it is inconvenient for the internal installation. The presence of them may alter the electric field distribution, resulting in potential breakdown of power equipment [1].

Recently, the fractal technique is introduced in antenna design. It provides not only desired miniaturization but also multiband performance [5]–[7]. The space-filling property can help lengthen the effective current path within the limited area; the self-similar property can aid the generation of multiple resonant modes. Presently, a variety of fractal geometries have been put forward, like Giuseppe Peano [5], Sierpinski carpet and gasket [6], and Koch snowflake [7]. These fractal geometries have certain limitations and drawbacks. For example, Peano fractal curve is too complex; Sierpinski fractal geometry can't be applied in the boundary but the interior of the radiation patch and ground plane; under the condition of the same iterative order, the bandwidth of Koch fractal antenna is narrower than that of Minkowski fractal antenna. In this work, a novel Minkowski fractal-based technique combined with complementary method is utilized to achieve both antenna miniaturization and bandwidth enhancement. It is

noteworthy that to the best of our knowledge, few literatures have investigated the influence of fractal direction on the impedance bandwidth so far, nevertheless, our work demonstrates that appropriate adjustment of the fractal direction can enhance the bandwidth.

This work is organized as follows: the structure of the proposed antenna is firstly described; then, the sensitivity analysis is performed to determine the influences of critical parameters on the impedance bandwidth. Furthermore, experiments have been conducted to confirm the theoretical analysis, and the return loss, radiation patterns, transfer function, and fidelity factors are measured. Finally, the electrical dimension and ratio bandwidth of the proposed antenna are compared with those of existing ones.

II. ANTENNA CONFIGURATION

The recursive procedure of Minkowski curve is illustrated in Fig. 1. Compared with square and regular hexagon, regular octagon has longer physical perimeter for given height. Hence, it is selected as the original structure of monopole. Figure 2 shows the application of Minkowski fractal geometry into the lateral boundaries of octagon.

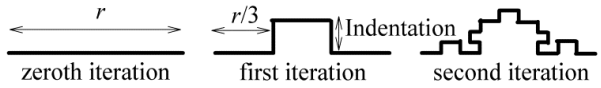

FIGURE 1. Recursive procedure of Minkowski curve.

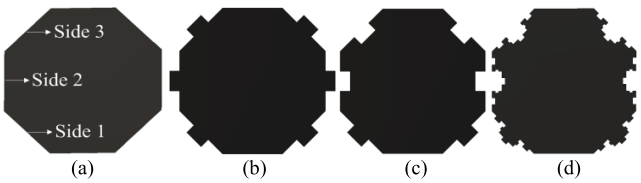

FIGURE 2. Application of Minkowski fractal geometry into the lateral boundaries of octagon. (a) Initiator. (b) All lateral sides are applied outward first-order fractal. (c) Side 1 is applied outward first-order fractal but sides 2 and 3 are applied inward first-order fractal. (d) Side 1 is applied outward second-order fractal but sides 2 and 3 are applied inward second-order fractal.

The geometry of the proposed antenna is depicted in Fig. 3. It is printed on FR4 substrate with dimension of 120 mm × 120 mm, $\varepsilon_r = 4.4$, and thickness = 1.6 mm. Here, the indentation factor, defined as the ratio of indentation depth to indentation length ($r/3$), is equal to 0.3; side 1 of octagon is applied outward second-order fractal whereas sides 2 and 3 are designed inward; the upper boundary of ground plane is applied the hybrid second-order fractal and it is cut a triangular notch below the feed line; three asymmetric strips are added at the top of fractal monopole. The photographs of this antenna are given in Fig. 4.

III. SENSITIVITY ANALYSIS

A. EFFECT OF ITERATIVE ORDER

Figure 5 shows the antenna structures of different iterative orders and fractal geometries, and the results are plotted

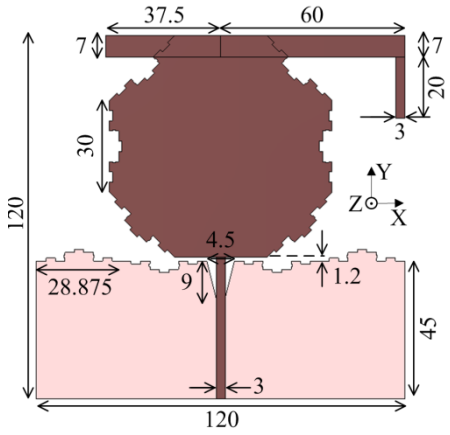

FIGURE 3. Geometry of proposed antenna (unit: millimeters).

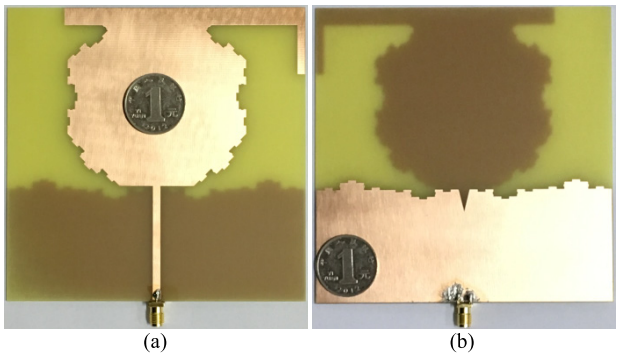

FIGURE 4. Photographs of proposed antenna. (a) Front view. (b) Back view.

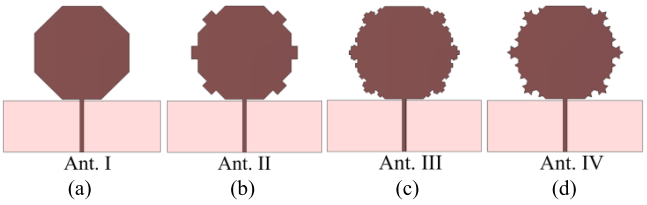

FIGURE 5. Antenna structures of different iterative orders and fractal geometries. (a) Original monopole. (b) Outward first-order Minkowski fractal. (c) Outward second-order Minkowski fractal. (d) Outward second-order Koch fractal.

in Fig. 6. As the iterative order increases, the low cutoff frequency (f_L) shifts toward the lower frequency band. However, the higher-order iteration makes the design and fabrication more complicated but will not significantly decrease f_L. Considering this aspect, the second iteration is applied in our work. Compared with existing second-order Koch fractal [7], the Minkowski fractal has wider impedance bandwidth.

B. EFFECT OF FRACTAL DIRECTION

Figures 7 gives the antenna structures of different fractal directions, and the results are plotted in Fig. 8. It indicates that bending side 1 of octagon inwards will lead to impedance mismatch at higher frequencies whereas the inward fractal of

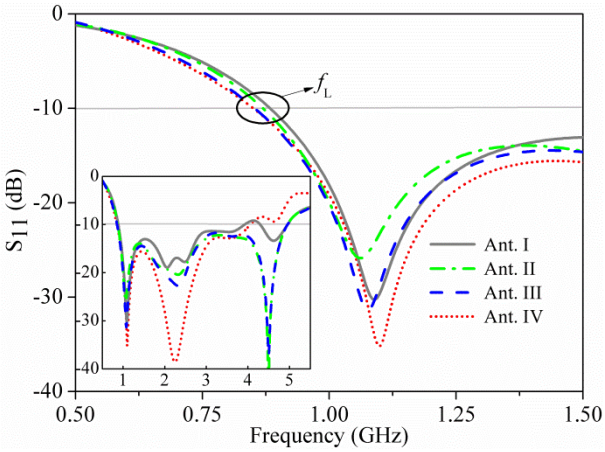

FIGURE 6. Influence of iterative order on impedance matching.

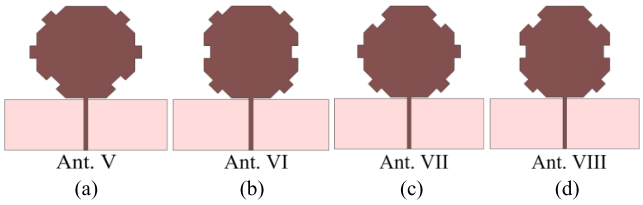

FIGURE 7. Antenna structures of different fractal directions. (a) Bending side 1 inwards and sides 2 and 3 outwards. (b) Bending side 2 inwards and sides 1 and 3 outwards. (c) Bending side 3 inwards and sides 1 and 2 outwards. (d) Bending sides 2 and 3 inwards and side 1 outwards.

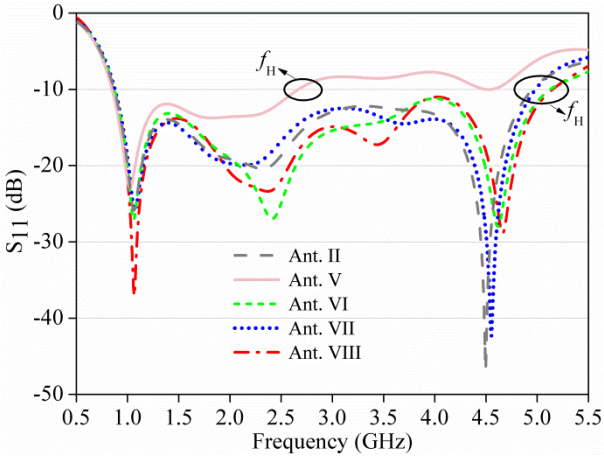

FIGURE 8. Influence of fractal direction on impedance matching.

either side 2 or 3 can raise the high cutoff frequency (f_H). Although the fractal direction is changed, the variation of f_L is negligible since the physical perimeter of monopole is kept the same.

C. EFFECT OF GROUND PLANE

The antenna structures of different ground planes are depicted in Fig. 9. From Fig.10, it can be found that the inward second-order fractal at the upper boundary of ground plane results in the decline of the first resonant frequency and low cutoff

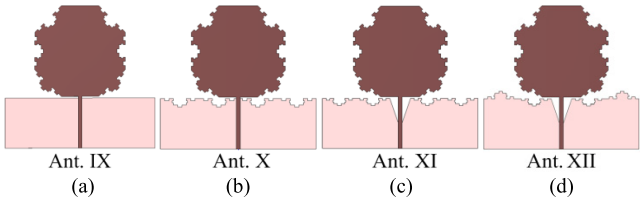

FIGURE 9. Antenna structures of different ground planes. (a) Without fractal. (b) Inward fractal without the triangular notch. (c) Inward fractal with the triangular notch. (d) Hybrid fractal with the triangular notch.

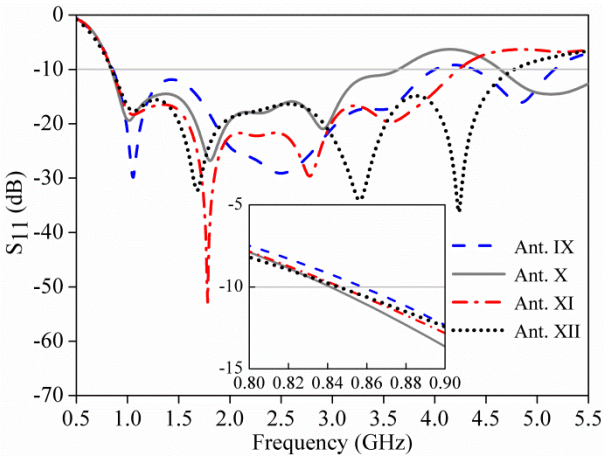

FIGURE 10. Influence of ground plane on impedance matching.

frequency. Compared to inward fractal, the hybrid fractal is more beneficial to enhance the impedance bandwidth. This is attributed to producing a quasi-self-complementary structure [8]. Additionally, cutting the triangular notch on the ground plane can significantly improve the impedance matching at higher frequencies [9].

D. EFFECT OF INDENTATION FACTOR

Figure 11 shows the impacts of indentation factor on the impedance bandwidth of Ant. XI. When the indentation factor

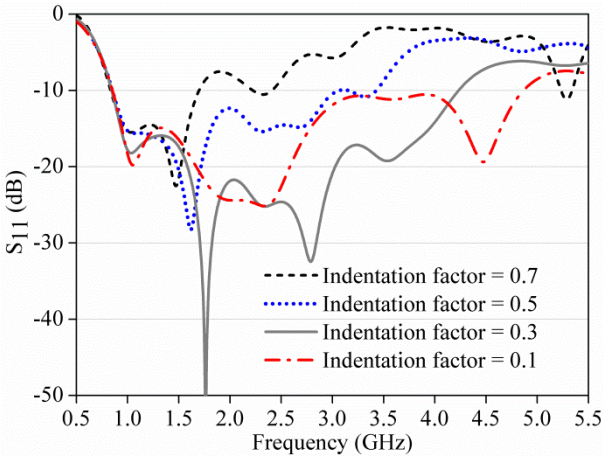

FIGURE 11. Influence of indentation factor on impedance bandwidth of Ant. XI.

equals 0.3, the antenna possesses wide impedance bandwidth and the most resonant depth. When the indentation factor exceeds an optimum value, the impedance bandwidth of antenna changes from wideband to multiband or narrowband. Similarly, the results can be obtained for Ant. XII.

E. EFFECT OF ASYMMETRIC STRIPS

The antenna structures of different strips are illustrated in Fig. 12. As the number of asymmetric strips increases, the low cutoff frequency shows a downward trend, whereas their reflection coefficients are almost identical in the frequency range of 4.0-5.5 GHz, as shown in Fig. 13.

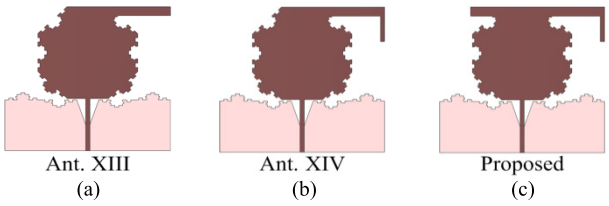

FIGURE 12. Antenna structures of different strips. (a) One strip. (b) Two strips. (c) Three strips.

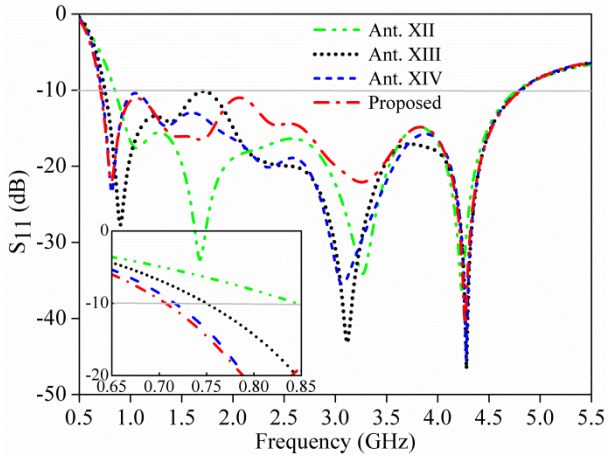

FIGURE 13. Influence of asymmetric strips on impedance matching.

TABLE 1. Simulated f_L, f_H, gain, and efficiency of evolutionary antennas.

Antenna	f_L (GHz)	f_H (GHz)	Gain (dBi)	Efficiency (%)
Ant. I	0.887	3.97	4.53	90.6
Ant. II	0.869	4.94	4.96	94.3
Ant. VIII	0.870	5.14	4.65	94.1
Ant. IX	0.857	4.00	4.46	93.1
Ant. X	0.841	3.63	4.27	93.4
Ant. XI	0.844	4.23	4.51	95.2
Ant. XII	0.845	4.78	4.75	95.0
Ant. XIII	0.755	4.80	4.71	94.9
Ant. XIV	0.717	4.80	4.79	95.4
Our work	0.708	4.80	4.47	95.1

Table 1 lists simulated f_L, f_H, gain and efficiency of the evolutionary antennas. Note that the gain and efficiency refer to the average peak gain and total efficiency in 10-dB return loss bandwidth, respectively. It can be observed that every evolution either decreases the low cutoff frequency or increases the high cutoff frequency, and all the evolutionary antennas have moderate gain and high efficiency. The f_L and f_H of the proposed antenna are 708 MHz and 4800 MHz, respectively. The former is declined by 20% than that of octagonal monopole whereas the latter is raised up by 21%.

IV. EXPERIMENTAL RESULTS

To validate the aforementioned analysis, a series of experiments have been conducted at an anechoic chamber of Gree Electric Appliances Inc.. The experimental setup consists of a diagonal dual polarization horn antenna, standard gain horn antennas, a multi-axis positioning system to rotate the test antenna, and a vector network analyzer (Keysight E5071C-280, bandwidth: 9 KHz - 8.5 GHz), etc.

Figure 14 gives the reflection coefficient of the proposed antenna. It demonstrates that experimental result agrees well with the simulation results. The discrepancy is minor throughout the entire frequency band. The frequency of $S_{11} < 10$-dB ranges from 700 to 4710 MHz, covering the major frequency spectrum of PD signal and fulfilling the requirement of impedance bandwidth for UHF antenna.

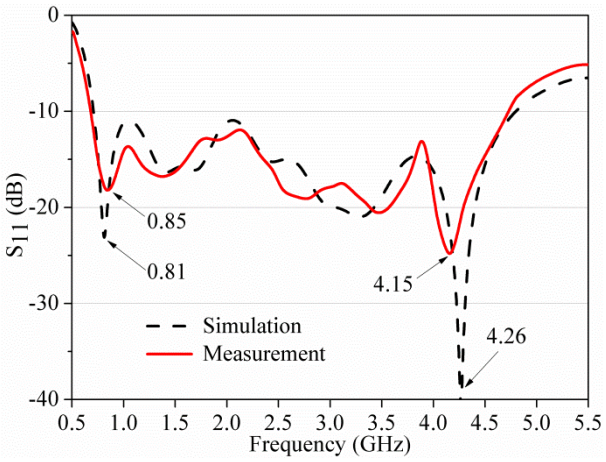

FIGURE 14. Reflection coefficient versus frequency.

Figure 15 presents the simulated surface current distribution at 0.81 and 4.26 GHz resonant frequencies. At both the frequencies, the current is mainly concentrated on the feed line, the edges of fractal monopole, the upper edges of ground plane, as well as the right strips. It indicates that the application of Minkowski fractal geometry and asymmetric strips can effectively increase the electrical length of antenna. Meanwhile, it can be found that the current density at 4.26 GHz is greater than that at 0.81 GHz. This is the reason why the resonant depth of the former is larger than that of the latter.

The radiation pattern of the proposed antenna is also measured in our work, as given in Fig. 16. Reasonable agreement between the simulated and measured results can be observed. In the XZ-plane, the radiation pattern is omnidirectional at 0.85 GHz, and the cross-polar component

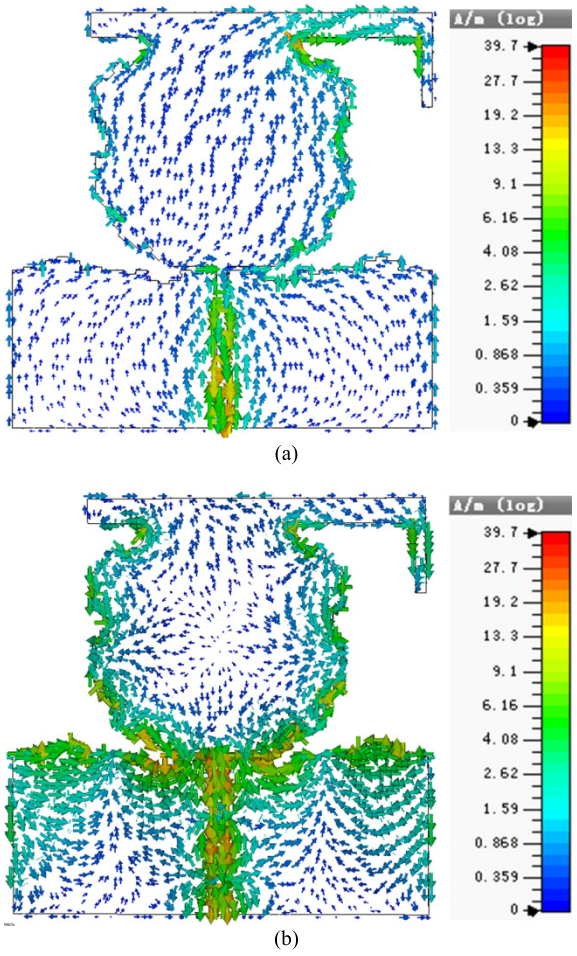

FIGURE 15. Simulated surface current distribution. (a) 0.81 GHz. (b) 4.26 GHz.

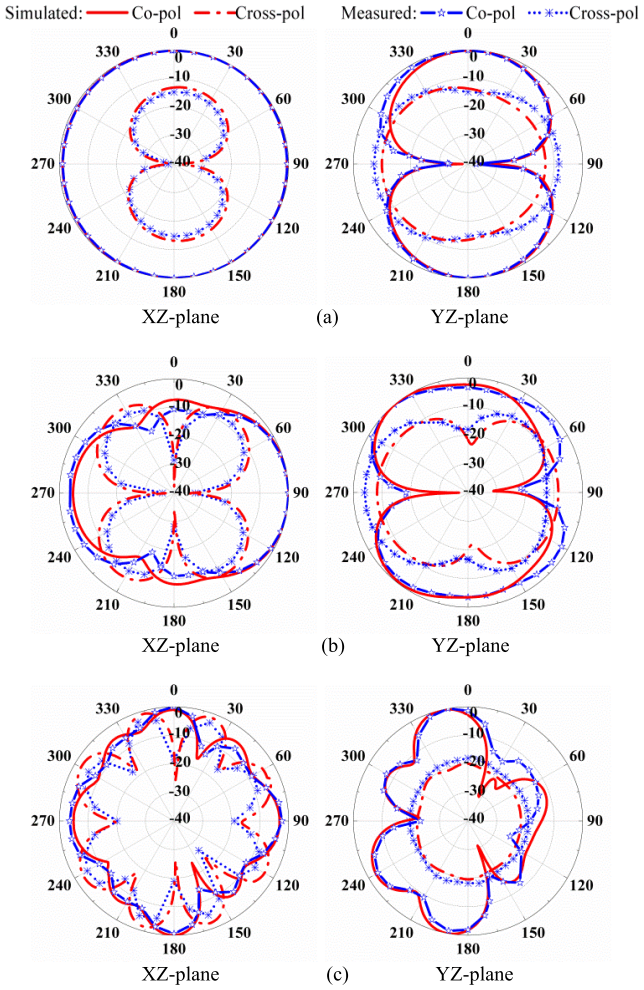

FIGURE 16. Radiation patterns. (a) 0.85 GHz. (b) 2.5 GHz. (c) 4.15 GHz.

increases to be comparable with the co-polar component at 2.5 and 4.15 GHz. Moreover, the gain in the right broadside direction is larger than that in the left side due to high current density congregating on the right strips. In the YZ-plane, both the co-polar and cross-polar components are relatively stable toward the lower and middle frequency bands, but the radiation pattern deteriorates slightly along with multiple lobes toward the higher frequency band.

Furthermore, the peak gain is measured from 700 MHz to 4.7 GHz with a step 200 MHz (see Fig. 17). Clearly, the measured gain is in good agreement with simulation results. The gain varies from 1.71 to 5.39 dBi, and the average value is about 3.93 dBi. In order to further improve the gain, antenna array can be adopted [1].

Regarding UWB antenna, the magnitude of transfer function should be as flat as possible and the phase response is required to keep linear in the band of interest [10], which accounts for constant group delay. The tests are carried out exploiting two same antennas with a distance of 1.5 m to comply with the far-field criteria. The measured transfer function is displayed in Fig. 18. The variation of S_{21} magnitude is less than 20 dB, the S_{21} phase is nearly linear, and the variation

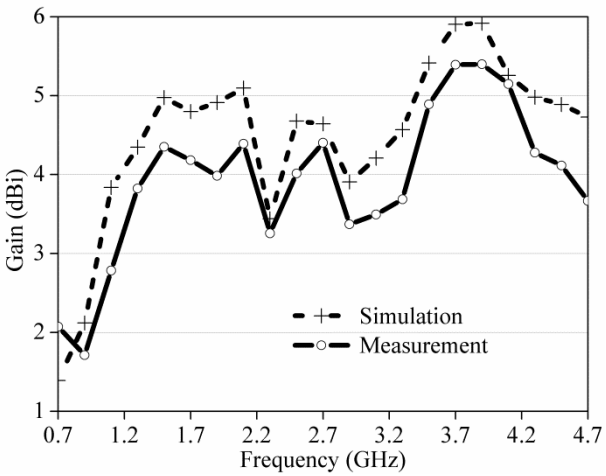

FIGURE 17. Peak gain versus frequency.

of group delay is less than 3 ns over the operating band. Therefore, the proposed antenna is relatively satisfactory for UWB applications.

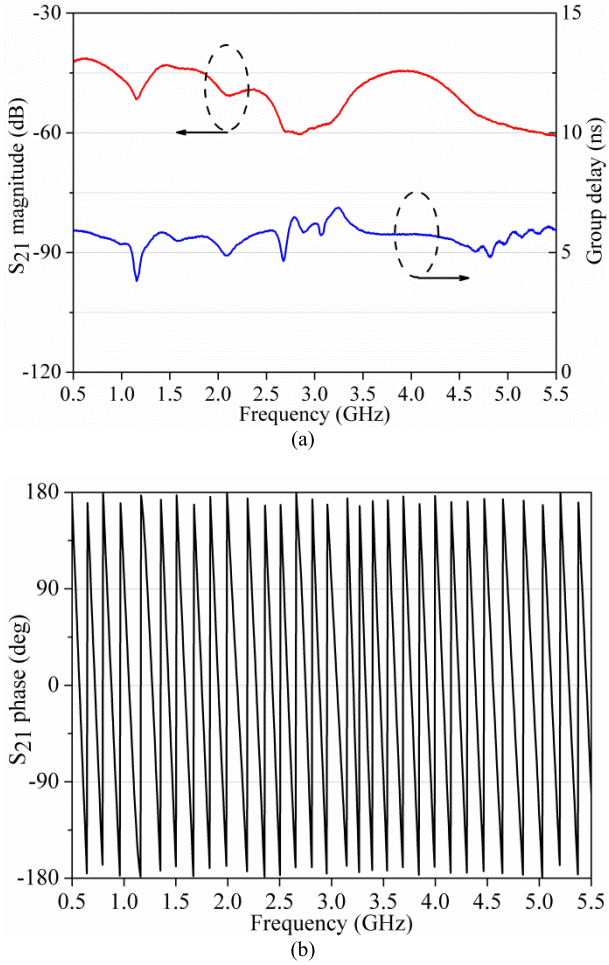

FIGURE 18. Measured transfer function. (a) S_{21} magnitude and group delay. (b) S_{21} phase.

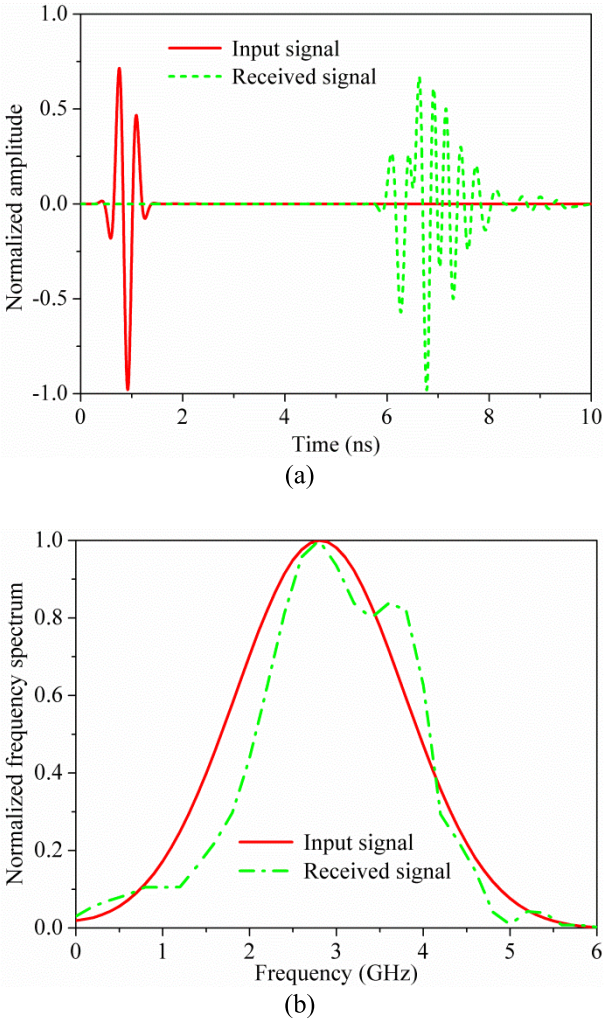

FIGURE 19. Normalized input signal and received signal in the face-to-face orientation. (a) Time domain. (b) Frequency domain.

In UHF detection system, the time-domain properties are as important as the frequency domain. According to the test plan suggested by [11], the receiver is rotated with a step 10° in the azimuthal plane whereas the transmitter is fixed. In order to increase the signal-to-noise ratio, a low-noise amplifier with 30 dB gain is added between the receiver and the vector network analyzer. The input signal adopts the default Gaussian pulse $S(t)$ of CST MWS software, the frequency spectrum of which covers the entire operating band of antenna. The measured received signal can be given by

$$R(t) = \mathrm{IFFT}\{\mathrm{FFT}[S(t)]\, S_{21}\} \tag{1}$$

where FFT and IFFT denote fast Fourier transform and inverse fast Fourier transform, respectively. Figure 19(a) presents the normalized input signal and received signal in the face-to-face orientation, with corresponding frequency spectrums in Fig. 19(b). In order to quantify the degree of similarity between the input signal and received signal, the fidelity factor, which is the only parameter that incorporates the time, space, and frequency together [11], is expressed as [12]

$$\rho = \max\{\frac{\int S(t)\, R(t+\tau)dt}{\sqrt{\int S^2(t)dt}\sqrt{\int R^2(t)dt}}\} \tag{2}$$

where τ is a delay that is varied to make the numerator in (2) maximum. Essentially, the fidelity factor is to characterize the correlation of two signals and in an ideal system without any distortion, the fidelity factor should be equal to 1 [13]. The calculated fidelity factors are plotted in Fig. 20. Here, 0° represents the face-to-face orientation. The minimum value is 0.71 occurring at 140° and the average value is 0.792. It indicates that the proposed antenna has good pulse handling capability.

In addition, the electrical dimension and ratio bandwidth of existing broadband antennas are summarized in Table 2. Here, λ_L is the wavelength in the free space at f_L. It can be observed that the proposed antenna has better compactness, excellent ratio of length to width, and wider bandwidth. Generally, there is a tradeoff between miniaturization and

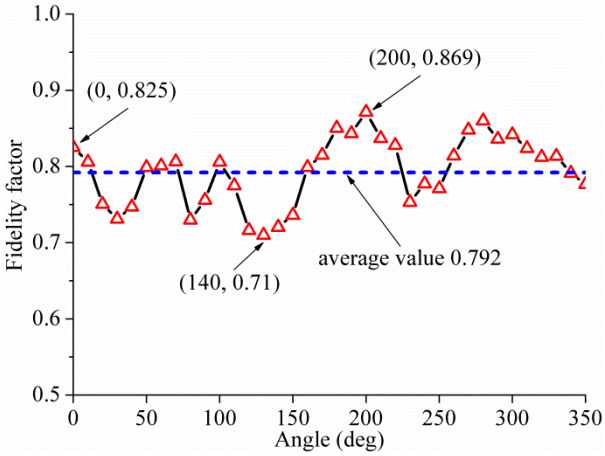

FIGURE 20. Fidelity factors in the azimuthal plane.

TABLE 2. Comparison of the proposed antenna with existing ones.

Ref.	Electrical dimension ($\lambda_L \times \lambda_L$)	Ratio bandwidth of $S_{11} < 10$-dB
[14]	0.210 × 0.210	1.67:1
[6]	0.457 × 0.457	1.93:1
[15]	0.275 × 0.275	2.40:1
[16]	0.301 × 0.326	2.90:1
[7]	0.351 × 0.317	3.82:1
[17]	0.377 × 0.403	4.41:1
[18]	0.294 × 0.252	4.60:1
[3]	0.509 × 0.509	> 5.00:1
[19]	0.518 × 0.266	13.51:1
[20]	0.440 × 0.440	13.64:1
Our work	0.280 × 0.280	6.72:1

impedance bandwidth. The proposed antenna is smaller in electrical size and its impedance bandwidth is larger than those in [6], [7], [16], and [17], especially, [6] is Sierpinski fractal slot antenna and [7] is Koch fractal antenna. Moreover, in the case of the same low cutoff frequency 700 MHz, the equiangular spiral antenna [3] needs extra microstrip impedance transformer to realize the impedance matching and the feed conversion from nonbalance to balance, resulting in the increase of overall height. Compared to the multiband Hilbert fractal UHF antenna whose maximum gain is about −28 dBi [21], the gain of our proposed antenna is higher; the 148% relative bandwidth of our proposed antenna is greater than the 34% relative bandwidth of Giuseppe Peano fractal antenna [5], which requires a layer of air gap between the radiation patch and ground plane. From the perspective of design and fabrication complexity, the proposed antenna is slightly more complicated than [5] and [6] but almost the same as [7] and [21].

V. CONCLUSION

The application of Minkowski fractal geometry and asymmetric strips to antenna design can extend the effective electrical length within limited space, thereby reducing the low cutoff frequency significantly without enlarging the size. Adjusting the fractal direction remarkably improves the impedance matching performance at higher frequency due to producing a complementary structure. The triangular notch forms a tapered feeding network, resulting in the enhancement of impedance bandwidth. The optimized antenna with size of $0.28\lambda_L \times 0.28\lambda_L$ has an impedance bandwidth of 0.7-4.71 GHz, good radiation patterns, moderate peak gain of average 3.93 dBi, and high fidelity factors. The proposed antenna can be also scaled for operating in the other band of PD signals, and it provides a solution to UHF detection.

REFERENCES

[1] J. Li, P. Wang, T. Jiang, L. Bao, and Z. He, "UHF stacked Hilbert antenna array for partial discharge detection," *IEEE Trans. Antennas Propag.*, vol. 61, no. 11, pp. 5798–5801, Nov. 2013.
[2] Y. Hai-Feng, Q. Yong, D. Yue, S. Ge-Hao, and J. Xiu-Chen, "Development of multi-band ultra-high-frequency sensor for partial discharge monitoring based on the meandering technique," *IET Sci., Meas., Technol.*, vol. 8, no. 5, pp. 327–335, Sep. 2014.
[3] T. Li, M. Rong, C. Zheng, and X. Wang, "Development simulation and experiment study on UHF partial discharge sensor in GIS," *IEEE Trans. Dielectr. Electr. Insul.*, vol. 19, no. 4, pp. 1421–1430, Aug. 2012.
[4] S. Kaneko, S. Okabe, M. Yoshimura, H. Muto, C. Nishida, and M. Kamei, "Detecting characteristics of various type antennas on partial discharge electromagnetic wave radiating through insulating spacer in gas insulated switchgear," *IEEE Trans. Dielectr. Electr. Insul.*, vol. 16, no. 5, pp. 1462–1472, Oct. 2009.
[5] H. Oraizi and S. Hedayati, "Miniaturization of microstrip antennas by the novel application of the Giuseppe Peano fractal geometries," *IEEE Trans. Antennas Propag.*, vol. 60, no. 8, pp. 3559–3567, Aug. 2012.
[6] Y. J. Sung, "Bandwidth enhancement of a wide slot using fractal-shaped Sierpinski," *IEEE Trans. Antennas Propag.*, vol. 59, no. 8, pp. 3076–3079, Aug. 2011.
[7] S. Tripathi, A. Mohan, and S. Yadav, "Hexagonal fractal ultra-wideband antenna using Koch geometry with bandwidth enhancement," *IET Microw., Antennas Propag.*, vol. 8, no. 15, pp. 1445–1450, 2014.
[8] L. Liu, S. W. Cheung, and T. I. Yuk, "Compact multiple-input–multiple-output antenna using quasi-self-complementary antenna structures for ultrawideband applications," *IET Microw. Antennas Propag.*, vol. 8, no. 13, pp. 1021–1029, Oct. 2014.
[9] L. Guo, S. Wang, X. Chen, and C. Parini, "A small printed quasi-self-complementary antenna for ultrawideband systems," *IEEE Antennas Wireless Propag. Lett.*, vol. 8, pp. 554–557, 2009.
[10] G.-P. Gao, B. Hu, and J.-S. Zhang, "Design of a miniaturization printed circular-slot UWB antenna by the half-cutting method," *IEEE Antennas Wireless Propag. Lett.*, vol. 12, pp. 567–570, 2013.
[11] G. Quintero, J.-F. Zurcher, and A. K. Skrivervik, "System fidelity factor: A new method for comparing UWB antennas," *IEEE Trans. Antennas Propag.*, vol. 59, no. 7, pp. 2502–2512, Jul. 2011.
[12] T. Kumar, A. K. Gautam, B. K. Kanaujia, and K. Rambabu, "Design of miniaturised UWB antenna for oil pipeline imaging," *Electron. Lett.*, vol. 51, no. 21, pp. 1626–1628, Oct. 2015.
[13] A. Amini, H. Oraizi, and M. A. C. Zadeh, "Miniaturized UWB log-periodic square fractal antenna," *IEEE Antennas Wireless Propag. Lett.*, vol. 14, pp. 1322–1325, 2015.
[14] S. A. Rezaeieh, A. Zamani, K. S. Bialkowski, and A. M. Abbosh, "Unidirectional slot-loaded loop antenna with wideband performance and compact size for congestive heart failure detection," *IEEE Trans. Antennas Propag.*, vol. 63, no. 10, pp. 4557–4562, Oct. 2015.
[15] Y. Sung, "Bandwidth enhancement of a microstrip line-fed printed wide-slot antenna with a parasitic center patch," *IEEE Trans. Antennas Propag.*, vol. 60, no. 4, pp. 1712–1716, Apr. 2012.
[16] H. Tang, K. Wang, R. Wu, and C. Yu, "Compact broadband CP monopole antenna with tilted branch," *Electron. Lett.*, vol. 52, no. 21, pp. 1739–1740, Oct. 2016.
[17] D. Aissaoui, L. M. Abdelghani, N. Boukli-Hacen, and T. A. Denidni, "CPW-fed UWB hexagonal shaped antenna with additional fractal elements," *Microw. Opt. Technol. Lett.*, vol. 58, no. 10, pp. 2370–2374, Oct. 2016.

[18] F. Wang, F. Bin, Q. Sun, J. Fan, F. Liang, and X. Xiao, "A novel UHF Minkowski fractal antenna for partial discharge detection," *Microw. Opt. Technol. Lett.*, vol. 59, no. 8, pp. 1812–1819, Aug. 2017.
[19] M. Yang, X. Yin, Y. Li, and L. Liu, "Ultra-wideband planar Gaussian tapered rhombic antenna for short pulse applications," *IEEE Antennas Wireless Propag. Lett.*, vol. 15, pp. 48–51, 2016.
[20] S. Cheng, P. Hallbjorner, and A. Rydberg, "Printed slot planar inverted cone antenna for ultrawideband applications," *IEEE Antennas Wireless Propag. Lett.*, vol. 7, pp. 18–21, 2008.
[21] J. Li, T. Jiang, C. Wang, and C. Cheng, "Optimization of UHF Hilbert antenna for partial discharge detection of transformers," *IEEE Trans. Antennas Propag.*, vol. 60, no. 5, pp. 2536–2540, May 2012.

FENG WANG received the B.Sc. degree from Xi'an Jiaotong University, Xi'an, China, in 1994, the M.Sc. degree from the Shenyang University of Technology, Shenyang, China, in 1999, and the Ph.D. degree from Xi'an Jiaotong University in 2003, all in electrical engineering. He is currently a Full Professor with Hunan University, Changsha, China. His research interests include antenna design, distribution network optimization and control, and high voltage engineering.

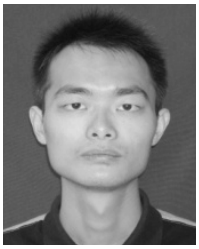

FENG BIN received the B.Sc. and M.Sc. degrees from the School of Physical and Electronic Science, Changsha University of Science and Technology, Changsha, China, in 2012 and 2015, respectively. He is currently pursuing the Ph.D. degree with the College of Electrical and Information Engineering, Hunan University, Changsha. His research interests include antenna design, partial discharge detection, pattern recognition, and signal processing.

QIUQIN SUN received the B.Sc. degree in electrical engineering from Chongqing University, Chonqing, China, in 2006, and the Ph.D. degree in electrical engineering from Shandong University, Jinan, China, in 2012. He is currently an Assistant Professor with Hunan University, Changsha, China. His research interests include antenna design and high voltage engineering.

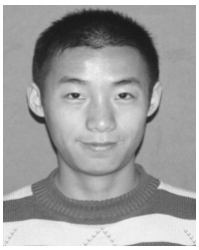

JINGMIN FAN received the B.Sc. and M.Sc. degrees in electronic science and technology from Central South University, Changsha, China, in 2007 and 2010, respectively. He is currently pursuing the Ph.D. degree in electrical engineering with Hunan University, Changsha. His research interests include antenna design, intelligent algorithm, and the state evaluation of power equipment.

HUISHENG YE received the B.Eng. and M.Eng. degrees in electrical engineering from the Huazhong University of Science and Technology, Wuhan, China, in 2004 and 2007, respectively. He is currently a Senior Engineer with the State Grid Hunan Electric Power Corporation Research Institute, Changsha, China. His research interests include antenna design and the state evaluation of power equipment.